The Journal of Immunology

ORAI1 Limits SARS-CoV-2 Infection by Regulating Tonic Type I IFN Signaling

Beibei Wu, Arunachalam Ramaiah, Gustavo Garcia, Jr., Spyridon Hasiakos, Vaithilingaraja Arumugaswami and Sonal Srikanth

J Immunol 2022; 208:74-84; Prepublished online 24 November 2021;
doi: 10.4049/jimmunol.2100742
http://www.jimmunol.org/content/208/1/74

The Journal of Immunology is published twice each month by
The American Association of Immunologists, Inc.,
1451 Rockville Pike, Suite 650, Rockville, MD 20852

Print ISSN: 0022-1767 Online ISSN: 1550-6606.

ORAI1 Limits SARS-CoV-2 Infection by Regulating Tonic Type I IFN Signaling

Beibei Wu,[*,1] Arunachalam Ramaiah,[†,‡,1] Gustavo Garcia, Jr.,[§] Spyridon Hasiakos,[*,¶] Vaithilingaraja Arumugaswami,[§,‖,#,2] and Sonal Srikanth[*,2]

ORAI1 and stromal interaction molecule 1 (STIM1) are the critical mediators of store-operated Ca^{2+} entry by acting as the pore subunit and an endoplasmic reticulum–resident signaling molecule, respectively. In addition to Ca^{2+} signaling, STIM1 is also involved in regulation of the type I IFN (IFN-I) response. To examine their potential role in severe acute respiratory syndrome coronavirus 2 (SARS-CoV-2) infection, we generated *ORAI1* and *STIM1* knockout human HEK293–angiotensin-converting enzyme 2 cells and checked their responses. *STIM1* knockout cells showed strong resistance to SARS-CoV-2 infection as a result of enhanced IFN-I response. On the contrary, *ORAI1* deletion induced high susceptibility to SARS-CoV-2 infection. Mechanistically, *ORAI1* knockout cells showed reduced homeostatic cytoplasmic Ca^{2+} concentration and severe impairment in tonic IFN-I signaling. Transcriptome analysis showed downregulation of multiple antiviral signaling pathways in *ORAI1* knockout cells, likely because of reduced expression of the Ca^{2+}-dependent transcription factors of the AP-1 family and *MEF2C*. Accordingly, modulation of homeostatic Ca^{2+} concentration by pretreatment with ORAI1 blocker or agonist could influence baseline *IFNB* expression and resistance to SARS-CoV-2 infection in a human lung epithelial cell line. Our results identify a novel role of ORAI1-mediated Ca^{2+} signaling in regulating the tonic IFN-I levels, which determine host resistance to SARS-CoV-2 infection. *The Journal of Immunology*, 2022, 208: 74–84.

Type I IFN (IFN-I) response provides the first line of defense against viral infection (1) and is also important for the development of adaptive immunity (2). IFN-I response is ubiquitous in almost all nucleated cells, whereas type III IFNs (IFN-IIIs) are restricted to anatomic barriers and specific immune cells (3). This selectivity is due to the receptor expression patterns: IFN-I binds IFN-α receptor 1 (IFNAR1) and IFNAR2, which are ubiquitously expressed, while IFN-III binds IFN-λ receptor 1 and L10RB, which are preferentially expressed in epithelial cells (3). Despite using different receptors, IFN-I and IFN-III activate the same downstream signaling pathways and induce transcription of hundreds of IFN-stimulated genes (ISGs), with IFN-III inducing lower levels of ISG expression than IFN-I (4). The importance of the IFN signaling pathway is underscored by the fact that most viruses have developed mechanisms to inactivate this pathway (5).

The coronavirus disease 2019 (COVID-19) pandemic is one of the worst crises of our times, prompting an urgent need to uncover host defense mechanisms to its causative agent, severe acute respiratory syndrome coronavirus 2 (SARS-CoV-2). SARS-CoV-2 uses multiple approaches to evade host IFN response, including suppression of IFN-I production and IFN-I signaling (6). The clinical manifestations and pathology of COVID-19 are similar to those of SARS-CoV-1, but the severities of the diseases differ (7). Unlike severe SARS-CoV-1 infection, SARS-CoV-2 infection shows a wide range of clinical features, ranging from asymptomatic to mild and moderate to severe and critical. The clinical manifestations of virus infection depend on virus–host interactions. Asymptomatic outcomes of SARS-CoV-2 infection may thus be attributed to strong host innate antiviral defense. In clinics, patients with COVID-19 with circulating Abs to IFN-I or loss-of-function mutations in genes necessary to mount the IFN-I response developed life-threatening

*Department of Physiology, David Geffen School of Medicine, University of California, Los Angeles, Los Angeles, CA; †Department of Ecology and Evolutionary Biology, University of California, Irvine, Irvine, CA; ‡Tata Institute for Genetics and Society, Center at inStem, Bangalore, Karnataka, India; §Department of Molecular and Medical Pharmacology, David Geffen School of Medicine, University of California, Los Angeles, Los Angeles, CA; ¶Division of Oral Biology and Medicine, UCLA School of Dentistry, Los Angeles, CA; ‖Eli and Edythe Broad Center of Regenerative Medicine and Stem Cell Research, University of California, Los Angeles, Los Angeles, CA; and #California NanoSystems Institute, University of California, Los Angeles, Los Angeles, CA

[1]B.W. and A.R. contributed equally to this work.

[2]V.A. and S.S. are cosenior authors.

ORCIDs: 0000-0003-3573-6141 (A.R.); 0000-0002-3034-095X (S.S.).

Received for publication July 29, 2021. Accepted for publication October 27, 2021.

This work was supported by the U.S. Department of Health and Human Services (HHS), National Institutes of Health (NIH), National Institute of Allergy and Infectious Diseases Grant AI146352 (to S.S.); HHS, NIH, National Eye Institute Grant EY032149 (to V.A.); National Institute of Diabetes and Digestive and Kidney Diseases Grant DK132735 (to V.A.), Broad Stem Cell Research Center institutional awards OCRC 20-76 (to S.S.) and OCRC 20-15 (to V.A.); and the California Institute for Regenerative Medicine Tran Award TRAN1COVID19-11975 (to V.A.). A.R. was supported by the Tata Institute for Genetics and Society.

S.S. conceptualized the study, generated KO cells, and performed imaging experiments. B.W. performed all the molecular biology and flow cytometry experiments, and A.R. performed bioinformatics analysis of the RNA sequencing data with help from S.H. G.G. and V.A. generated the severe acute respiratory syndrome coronavirus 2 virus and performed all infection experiments. S.S. wrote the manuscript with input from all authors.

The RNA sequencing data have been submitted to the National Center for Biotechnology Information Gene Expression Omnibus (https://www.ncbi.nlm.nih.gov/geo/query/acc.cgi?acc=GSE173707) under accession number GSE173707.

Address correspondence and reprint requests to Dr. Sonal Srikanth or Dr. Vaithilingaraja Arumugaswami, Department of Physiology, David Geffen School of Medicine, 53-266 CHS, 10833 Le Conte Avenue, Los Angeles, CA 90095 (S.S.) or Department of Molecular and Medical Pharmacology, David Geffen School of Medicine, University of California, Los Angeles, B2-049A CHS, Box 956948, Los Angeles, CA 90095 (V.A.). E-mail addresses: ssrikanth@mednet.ucla.edu (S.S.) or varumugaswami@mednet.ucla.edu (V.A.).

The online version of this article contains supplemental material.

Abbreviations used in this article: ACE2, angiotensin-converting enzyme 2; $[Ca^{2+}]$, Ca^{2+} concentration; $[Ca^{2+}]_i$, intracellular Ca^{2+} concentration; COVID-19, coronavirus disease 2019; CRAC, Ca^{2+} release-activated Ca^{2+}; CsA, cyclosporine A; C_T, threshold cycle; DEG, differentially expressed gene; ER, endoplasmic reticulum; FDR, false discovery rate; HSV-1, HSV type 1; IFNAR1, IFN-α receptor 1; IFN-I, type I IFN; IRF, IFN regulatory factor; ISG, IFN-stimulated gene; KO, knockout; MOI, multiplicity of infection; Pen/Strep, penicillin/streptomycin; PRDI, positive regulatory domain I; RNA-seq, RNA sequencing; SARS-CoV-2, severe acute respiratory syndrome coronavirus 2; sgRNA, single guide RNA; SOCE, store-operated Ca^{2+} entry; STIM1, stromal interaction molecule 1; STING, stimulator of IFN genes.

pneumonia (8, 9). Recent studies have found that unlike original coronaviruses, SARS-CoV-2 is highly sensitive to pretreatment with type I and III IFNs. Pretreatment of immortalized or primary human airway epithelial cells with IFN-I or IFN-III imparts resistance to SARS-CoV-2 infection (10–12). Further, recent studies aiming at boosting IFN-I signaling, via pharmacological activation of stimulator of IFN genes (STING), robustly inhibited infection of multiple coronaviruses, including SARS-CoV-2 in vitro and in vivo (13–16). Taken together, a picture emerges that tonic IFN-I signaling mediated by the baseline levels of IFN-I, which is known to prime the host antiviral status (17), can also provide a significant barrier to SARS-CoV-2 infection.

Store-operated Ca^{2+} entry (SOCE), induced by depletion of the endoplasmic reticulum (ER) Ca^{2+} stores after activation of G protein–coupled receptors or receptor tyrosine kinases, is a ubiquitous mechanism of elevation of intracellular Ca^{2+} concentration ($[Ca^{2+}]_i$) in most cell types. Ca^{2+} release-activated Ca^{2+} (CRAC) channels are a specialized class of store-operated Ca^{2+} channels that play a primary role in the elevation of $[Ca^{2+}]$ in immune cells (18, 19). CRAC channels consist of two major components: the plasma membrane–localized pore subunit, ORAI1; and an ER-resident Ca^{2+} sensor, stromal interaction molecule 1 (STIM1). STIM1 senses depletion of the ER Ca^{2+} stores and interacts with ORAI1 to open the pore. Ca^{2+} signaling mediated by CRAC channels is essential for induction of transcriptional programs via the NFAT pathway (18, 19). Severe combined immune deficiency caused by mutations in *ORAI1* or *STIM1*, and the widespread clinical use of inhibitors of this pathway, cyclosporine A (CsA) and FK506, as immunosuppressants underscore the importance of therapeutic targeting of the Ca^{2+}-NFAT pathway (18, 19).

Although the current understanding of the role of ORAI1 is limited to Ca^{2+} signaling, a Ca^{2+} signaling–independent role of STIM1 in regulating the IFN-I response has been shown (20). Biochemical studies identified STIM1 as an interacting partner of STING, an ER-resident adaptor protein that plays a central role in cellular response to cytosolic DNA (21). It was shown that STIM1 forms a complex with STING on the ER membrane to prevent its aberrant activation in an SOCE-independent manner. Myeloid cell–specific *Stim1* knockout (KO) mice and a patient lacking STIM1 expression were shown to have elevated serum IFN-β and increased expression of various ISGs (20, 22). Accordingly, myeloid-specific *Stim1* KO mice showed enhanced resistance to DNA virus infection, which was not observed in *Orai1* KO cells and mice (20). In this study, we examined the role of *ORAI1* and *STIM1* in host resistance to infection with an RNA virus, SARS-CoV-2. Loss of ORAI1 markedly reduced the host resistance to SARS-CoV-2 by abolishing the baseline IFN-β levels and impairing tonic IFN-I signaling. On the contrary, *STIM1* KO cells showed remarkable resistance to SARS-CoV-2 infection, supporting previous studies of enhanced baseline IFN-I signaling (20). Our data suggest that tonic IFN-I signaling regulated by ORAI1 and STIM1 determines the cellular antiviral state and host resistance to SARS-CoV-2 infection.

Materials and Methods

Chemicals and Abs

Fura 2-AM (F1221) was purchased from Thermo Fisher Scientific. Thapsigargin and cyclosporin A were purchased from EMD Millipore. SARS-CoV Spike (S) Ab, polyclonal anti-SARS coronavirus (BEI Resources: NR-10361 antiserum, Guinea Pig), was used for immunoblotting, and monoclonal anti-SARS-CoV S protein Ab (BEI Resources: NR-616, similar to 240C) was used for immunocytochemistry (ICC). Abs for detection of human STIM1 (5668S) were purchased from Cell Signaling Technologies, Abs for detection of IFNAR1 and IFN-β receptor 1 were purchased from Leinco Technologies (I-400), Abs for detection of ORAI1 (ACC-060) were purchased from Alomone Labs, and Abs for detection of β-actin (sc-47778) were obtained from Santa Cruz Biotechnology. BTP2 and ionomycin were purchased from Millipore Sigma.

Plasmids, single guide RNAs, and cells

The human angiotensin-converting enzyme 2 (ACE2) coding sequence was cloned into a lentiviral vector as described previously (23). Single guide RNAs (sgRNAs) targeting human *ORAI1* (guide RNA target sequence 5′-GATCGG CCAGAGTTACTCC-3′) and human *STIM1* (5′-TGAGGATAAGCTCAT-CAGCG-3′) genes were subcloned into pLentiguide puro (Addgene). sgRNAs targeting human IFNAR1 and IFN-β receptor 1 subcloned into pLentiCRISPR v2 were purchased from GenScript (catalog no. IFNAR1 crRNA 1; guide RNA target sequence 5′-GGCGTGTTTCCAGACTGTTT-3′). Vero E6, HEK293, and A549 cells were obtained from the American Type Culture Collection center (ATCC, Manassas, VA). Vero cells were cultured in Eagle's MEM growth media (ATCC) supplemented with 10% (v/v) FBS (Hyclone) and penicillin/streptomycin (Pen/Strep; Mediatech) at 37°C and 5% CO_2. HEK293 cells were cultured in DMEM (Mediatech) supplemented with 10% (v/v) FBS (Hyclone), 2 mM L-glutamine (Mediatech), 10 mM HEPES (Mediatech), and Pen/Strep (Mediatech) at 37°C and 5% CO_2. A549 cells were cultured in Ham's F12-K (Kaighn's) medium (Thermo Fisher) supplemented with 10% (v/v) FBS (Hyclone), 10 mM HEPES (Mediatech), and Pen/Strep (Mediatech) at 37°C and 5% CO_2.

Virus

SARS-CoV-2 (USA-WA1/2020) was obtained from BEI Resources of National Institute of Allergy and Infectious Diseases. All the studies involving live virus were conducted in the UCLA BSL3 high-containment facility. SARS-CoV-2 was passaged once in Vero E6 cells, and viral stocks were aliquoted and stored at −80°C. Virus titer was measured in Vero E6 cells by established plaque assays.

Lentiviral transduction of HEK293 and A549 cells

To generate HEK293-ACE2 or A549-ACE2 cells, we transfected HEK293T cells with plasmid encoding ACE2 and packaging vectors (pMD2.G and psPAX2; Addgene) using calcium phosphate transfection method. Culture supernatants were harvested at 48 and 72 h posttransfection, filtered using a 0.45-μm polyvinylidene difluoride filter, and used for infection of HEK293 or A549 cells together with polybrene (8 μg/ml) using the spin-infection method. Transduced cells were selected with puromycin (1 μg/ml) 48 h after a second infection. For generation of $ORAI1^{-/-}$ and $STIM1^{-/-}$ cells, HEK293T cells were transfected with plasmids encoding sgRNA and packaging vectors as described earlier. Lentiviruses encoding Cas9 were generated using the same technique. Culture supernatants harvested at 48 and 72 h posttransfection were used for infection (50% of Cas9-encoding virus + 50% of sgRNA-encoding virus) of HEK293-ACE2 or A549-ACE2 cells together with polybrene (8 μg/ml) using the spin-infection method. Cells were selected with puromycin (1 μg/ml) and blasticidin (5 μg/ml) 48 h after the second infection.

Endogenous ORAI1 staining and analysis

For total endogenous ORAI1 detection, control, STIM1 KO, and ORAI1 KO HEK293 (0.5×10^6) were fixed with 4% paraformaldehyde at room temperature for 15 min, followed by permeabilization with PBS + 0.5% Igepal CA-630, and incubated with 1 μg unlabeled anti-ORAI1 Ab (ACC-060; Alomone laboratories) in PBS + 2% FBS + 0.5% Igepal CA-630. Negative control sample did not contain the primary Ab. Cells were subsequently treated with FITC-conjugated secondary Ab, washed, and data were acquired on a BD Fortessa flow cytometer (BD Biosciences) and analyzed using FlowJo software (Tree Star).

Single-cell Ca^{2+} imaging and immunofluorescence analysis

HEK293-ACE cells were grown overnight on coverslips and loaded with 1 μM Fura 2-AM for 40 min at 25°C for imaging. $[Ca^{2+}]_i$ measurements were performed using essentially the same methods as previously described (24). In brief, microscopy was performed using an Olympus IX2 illumination system mounted on an Olympus IX51 inverted microscope using previously described methods (25). Acquisition and image analysis were performed using Slidebook (Intelligent Imaging Innovations) software, and graphs were plotted using Origin2020 (OriginLab). For immunofluorescence analysis, uninfected or SARS-CoV-2–infected cells were fixed for 20 min with ice-cold methanol, permeabilized in buffer containing PBS + 0.2% Triton X-100, and blocked with the same buffer containing 2.5% goat serum, 2.5% donkey serum, and 2% BSA. Cells were stained overnight in the blocking buffer with primary Abs washed and treated with secondary Ab for 1 h, stained for DAPI in permeabilization solution, visualized using 40× oil

immersion lens, and imaged using Slidebook 6.0 software (Intelligent Imaging Innovations). Images were processed for enhancement of brightness or contrast using Slidebook 6.0 software.

SARS-CoV-2 infection

Control, *ORAI1*$^{-/-}$, or *STIM1*$^{-/-}$ HEK293-ACE2 cells or A549-ACE2 cells were seeded at 1×10^5 cells/well in 0.4 ml vol in a 48-well plate, or 5×10^4 cells/well in 0.2 ml vol in a 96-well plate. The following day, viral inoculum (multiplicities of infection [MOIs] of 0.1 or 1.0 as indicated) was prepared using serum-free media. The spent media from each well were removed, and 100 μl of prepared inoculum was added onto cells. For mock infection, serum-free media (100 μl/well) alone were added. The inoculated plates were incubated for 1 h at 37°C with 5% CO_2. The inoculum was spread by gently tilting the plate sideways every 15 min. At the end of incubation, the inoculum was replaced with serum-supplemented media. At 20 h postinfection, the cells were either fixed with methanol for ICC analysis, harvested in TRIzol reagent (Thermo Fisher) for RNA sequencing (RNA-seq) and RT-PCR analysis, or lysed in radioimmunoprecipitation assay lysis buffer for immunoblotting as described later.

Plaque assay

Viral titers were determined by plaque assay on Vero E6 cells. Vero E6 cells were seeded in 12-well plates for 24 h. Virus-containing supernatants were 10-fold serially diluted in PBS. The growth medium was removed from the cells, cells were washed once with PBS, and diluted supernatants were added (150 μl/well). After 30-min inoculation, an overlay medium (double-concentrated MEM [supplemented with 2% L-glutamine, 2% Pen/Strep, 0.4% BSA], mixed 1:1 with 2.5% Avicel solution [prepared in ddH_2O]) was added to the cells (1.5 ml/well). Then, cells were incubated for 72 h at 37°C. After 72 h, the overlay medium was removed from the cells, and after a washing step with 1× PBS, the cells were fixed with 4% paraformaldehyde for 30 min at 4°C. Subsequently, the cells were counterstained with crystal violet solution to visualize the virus-induced plaques in the cell layer. The number of plaques at a given dilution was counted to calculate the viral titers as PFUs (PFUs/ml).

RNA sample preparation and real-time quantitative PCR

Total RNA from cells harvested in TRIzol Reagent (Thermo Fisher) was isolated using the Direct-zol RNA isolation kit (Zymo Research). RNA quantity and quality were confirmed with a NanoDrop ND-1000 spectrophotometer. cDNA was synthesized using 0.5–1.0 μg of total RNA using random hexamers and oligo(dT) primers and qScript cDNA Supermix (Quantabio). Real-time quantitative PCR was performed using iTaq Universal SYBR Green Supermix (Bio-Rad) and an iCycler IQ5 system (Bio-Rad) using gene-specific primers. In brief, amplification was performed using 20-μl vol reactions in a 96-well plate format with the following conditions: 95°C for 30 s for polymerase activation and cDNA denaturation, then 40 cycles at 95°C for 15 s and 60°C for 1 min, with a melt-curve analysis at 65°C–95°C and 0.5°C increments at 2–5 s/step. Threshold cycles (C_T) for all the candidate genes were normalized to those of 36B4 to obtain ΔC_T. The specificity of primers was examined by melt-curve analysis and agarose gel electrophoresis of PCR products. Primer sequences are as follows: *SARS-CoV-2* (forward: 5′-GACCCCAAAATCAGCGAAAT-3′, reverse: 5′-TCTGGTTACTGCCAGTTGAATCTG-3′), human *ATF2* (forward: 5′-GCACAGCCCACATCAGCTATT-3′, reverse: 5′-GGTGCCTGGGTGATTACAGT-3′); human *FOS* (forward: 5′-GGGGCAAGGTGGAACAGTTAT-3′, reverse: 5′-CCGCTTGGAGTGTATCAGTCA-3′); human *MEF2C* (forward: 5′-GTATGGCAATCCCCGAAACT-3′, reverse: 5′-ATCGTATTCTTGCTGCCTGG-3′), and human *36B4* (forward: 5′-AGATGCAGCAGATCCGCAT-3′, reverse: 5′-GTTCTTGCCCATCAGCACC-3′).

Western blot analysis

Cells were lysed in radioimmunoprecipitation assay lysis buffer (50 mM Tris [pH 7.4], 1% Nonidet P-40, 0.25% sodium deoxycholate, 1 mM EDTA, 150 mM NaCl, 1 mM Na_3VO_4, 20 mM NaF, 1 mM PMSF, 2 mg/ml aprotinin, 2 mg/ml leupeptin, and 0.7 mg/ml pepstatin) for 1 h with intermittent vortexing and centrifuged to remove debris. Samples were separated on 10% SDS-PAGE. Proteins were transferred to nitrocellulose membranes and subsequently analyzed by immunoblotting with relevant Abs. Chemiluminescence images were acquired using an Image reader LAS-3000 LCD camera (FujiFilm).

Cytokine measurement by ELISA

For ELISA measurements under resting conditions, 1 million cells were cultured in low media volume to allow for concentration of cytokines. ELISA was performed on cell culture supernatants from indicated cells for detection of IFN-β (#41410; PBL Assay Science) or IL-6 (#88-7066-22; Thermo Fisher Scientific) using the manufacturer's instructions.

RNA-seq and data analysis

RNA was extracted with Direct-zol RNA Mini prep kit (Zymo Research). Libraries for RNA-seq were prepared with TruSeq Stranded mRNA Library Prep Kit (Illumina). The workflow consisted of mRNA enrichment and fragmentation. Cleaved RNA fragments were copied into first-strand cDNA using reverse transcriptase and random primers. Strand specificity is achieved by replacing dTTP with deoxyuridine triphosphate, followed by second-strand cDNA synthesis using DNA Polymerase I and RNase H. cDNA generation is followed by A-tailing, adaptor ligation, and PCR amplification. Different adaptors were used for multiplexing samples in one lane. Sequencing was performed on Illumina HiSeq 3000 for SE 1 × 50 run. Data quality check was done on Illumina SAV. Demultiplexing was performed with Illumina Bcl2fastq v2.19.1.403 software. Raw reads for Orai1KO and STIM1KO SARS-CoV-2–infected samples (Orai1KO-SARS-CoV-2-3_S18 and STIM1KO-SARS-CoV-2-1_S19) were sampled down to 45 million reads before mapping. Illumina reads from all samples were mapped to human and SARS-CoV-2 reference genomes by STAR v2.27a (26), and read counts per gene were quantified using human Ensembl GRCh38.98 and SARS-CoV-2 GTF file to generate raw reads counts. Differential expression analysis was performed using DESeq2 v1.28.1 in R v4.0.3 (27). Median of ratios method was used to normalize expression counts for each gene in all experimental samples. Each gene in the samples was fitted into a negative binomial generalized linear model. Differentially expressed gene (DEG) candidates were considered if they were supported by a false discovery rate (FDR) $p < 0.01$. Unsupervised principal component analysis was performed using pcaExplorer (28) in R v4.0.3 (27). Reactome pathway analysis was performed for DEGs using all human genes as reference dataset in the Reactome v65 (29) implemented in PANTHER. Reactome pathways were considered only if they were supported by FDR $p < 0.05$. The ggplot2 v3.3.2 in R and Prism GraphPad v8.4.3 were used to generate figures. The shinyheatmap web interface was used to prepare heatmaps (30). The genes in the DEGs directly regulated by transcription factors (*FOS*, *ATF2*, *MEF2C*, and *JUN*) were identified based on binding profiles of all public ChIP-seq data for particular gene loci from the ChIP-Atlas database (31). The regulated or target genes were accepted if the peak-call intervals of a given gene overlapped with a transcription start site ±1 kb. RNA-seq data have been deposited to the NCBI GEO under the accession number GSE173707 (https://www.ncbi.nlm.nih.gov/geo/query/acc.cgi?acc=GSE173707).

Statistical analysis

Statistical analysis was carried out using two-tailed Student *t* test. Differences were considered significant when *p* values were <0.05. The hypergeometric test in R v4.0.3 was used to measure the statistical significance of the enriched genes in the DEGs regulated by transcription factors (*FOS*, *ATF2*, *MEF2C*, and *JUN*) compared with regulated genes in the background gene sets of the human reference genome.

Results

Loss of ORAI1 reduces SOCE and the baseline cytoplasmic [Ca^{2+}] in HEK293-ACE2 cells

To examine the role of ORAI1 and STIM1 in host response to SARS-CoV-2, we generated HEK293 cells stably expressing the receptor for SARS-CoV-2, ACE2 (32). The resulting HEK293-ACE2 cells were transduced with lentiviruses encoding Cas9 and sgRNAs targeting either *ORAI1* or *STIM1*. All three lines expressed similar levels of ACE2 as judged by ICC and immunoblotting (Supplemental Fig. 1A, 1B). Loss of STIM1 protein expression was validated by immunoblotting, while that of ORAI1 was validated by flow cytometry (Fig. 1A, 1B). Multiple studies have shown loss of SOCE in HEK293 cells deleted for expression of *ORAI1*/*STIM1* (33, 34). To measure SOCE in *ORAI1*$^{-/-}$ and *STIM1*$^{-/-}$ HEK293-ACE2 cells, we used thapsigargin, a blocker of sarcoplasmic reticulum/ER Ca^{2+}-ATPase pump, that allows for passive depletion of the ER Ca^{2+} stores, thereby activating SOCE. We observed almost complete abrogation of SOCE in both *ORAI1*$^{-/-}$ and *STIM1*$^{-/-}$ HEK293-ACE2 cells (Fig. 1C). Although control cells showed a uniform increase in SOCE after reintroducing Ca^{2+}-containing Ringer's solution, more than 95% of the polyclonal *ORAI1*$^{-/-}$ and *STIM1*$^{-/-}$ HEK293-ACE2 cells remained unresponsive. The Ca^{2+} release from the ER in those cells was similar. Next, we checked whether loss of ORAI1/STIM1

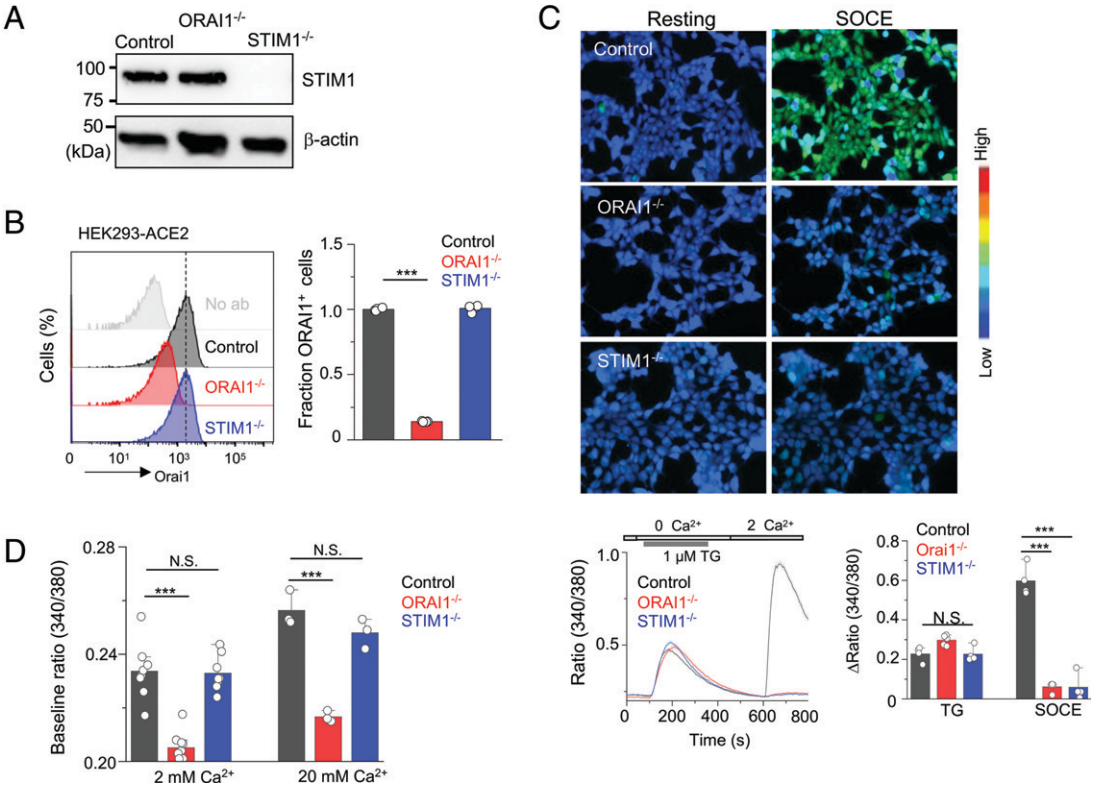

FIGURE 1. Loss of ORAI1 reduces basal Ca^{2+} concentration and abrogates SOCE in HEK293-ACE2 cells. (**A**) Representative immunoblot showing expression of STIM1 in lysates from control, *ORAI1*$^{-/-}$, or *STIM1*$^{-/-}$ HEK293-ACE2 cells. β-Actin is the loading control. Data are representative of two independent experiments. (**B**) Representative histograms showing levels of total ORAI1 protein in control, *ORAI1*$^{-/-}$, and *STIM1*$^{-/-}$ HEK293-ACE2 cells after permeabilization and intracellular staining with anti-ORAI1 Ab. The bar graph shows average (± SEM) from three independent experiments. (**C**) Representative pseudocolored epifluorescence images (original magnification ×200) of indicated cells under resting conditions or at the peak of SOCE. (Bottom) Representative traces showing averaged SOCE from control (39 cells), *ORAI1*$^{-/-}$ (35 cells), and *STIM1*$^{-/-}$ (42 cells) HEK293-ACE2 cells after passive depletion of intracellular Ca^{2+} stores with thapsigargin (TG; 1 μM) in Ca^{2+}-free external solution. SOCE was measured after replacing external solution with that containing 2 mM $CaCl_2$. Bar graph on the right shows averaged baseline subtracted ER Ca^{2+} stores (TG) and SOCE (± SEM) from four independent experiments. (**D**) Bar graph shows baseline Ca^{2+} levels (as depicted by Fura-2 ratio) ± SEM in indicated cell types upon perfusion with extracellular solution containing either 2 or 20 mM $CaCl_2$. Each dot represents data obtained from an independent experiment. ***$p < 0.0005$ (two-tailed *t* test).

affected resting cytoplasmic [Ca^{2+}] in unstimulated cells. Using our previously established protocols, we sequentially perfused the cells with 0 (Ca^{2+}-free), 2, and 20 mM Ca^{2+}-containing Ringer's solutions without any store depletion, to measure the homeostatic Ca^{2+} levels in cells (25). Interestingly, in these measurements, only *ORAI1*$^{-/-}$ HEK293-ACE2 cells showed significant reduction in baseline [Ca^{2+}] in the presence of 2 or 20 mM Ca^{2+}-containing Ringer's solution, suggesting an additional role of ORAI1 in regulating homeostatic [Ca^{2+}] in these cells (Fig. 1D). These data are in concurrence with previous observations where STIM2, a homolog of STIM1, was shown to be involved in maintaining resting $[Ca^{2+}]_i$ together with ORAI1 (35). In those experiments, STIM2-depleted cells showed decreased resting $[Ca^{2+}]_i$, while those depleted for STIM1 had normal levels of resting $[Ca^{2+}]_i$. Collectively, by stable expression of ACE2 and deletion of *ORAI1*/*STIM1*, we developed a system to examine the role of ORAI1 and STIM1 in host responses to SARS-CoV-2 infection and uncovered the role of ORAI1 in Ca^{2+} homeostasis in these cells.

Loss of ORAI1 and STIM1 affects host resistance to SARS-CoV-2 infection

Next, we infected control, *ORAI1*$^{-/-}$, and *STIM1*$^{-/-}$ HEK293-ACE2 cells with SARS-CoV-2 at two different MOIs, – 0.1 and 1.0. Twenty hours postinfection, cells were harvested to examine expression of viral proteins, as well as quantification of viral genome. We observed high levels of viral protein expression in SARS-CoV-2–infected *ORAI1*$^{-/-}$ HEK293-ACE2 cells when compared with control cells by immunoblotting (Fig. 2A), such that 20 h postinfection at high MOI (1.0), a significant fraction of the *ORAI1*$^{-/-}$ cells was lysed (Fig. 2B). On the contrary, *STIM1*$^{-/-}$ HEK293-ACE2 cells showed strong resistance to SARS-CoV-2 infection as judged by markedly reduced expression of viral protein by immunoblotting and fewer plaques by ICC when compared with control cells (Fig. 2A, 2B). Genome copy measurements at 5 h postinfection showed modestly increased and decreased susceptibility of *ORAI1*$^{-/-}$ and *STIM1*$^{-/-}$ cells, respectively, especially in cells infected at high MOI (Fig. 2C, left). Further, the increased and decreased susceptibility of *ORAI1*$^{-/-}$ and *STIM1*$^{-/-}$ cells, respectively, were obvious at 20 h postinfection, where *ORAI1*$^{-/-}$ cells showed an ∼100-fold increase in viral genome copy numbers, whereas *STIM1*$^{-/-}$ cells showed more than 100-fold reduction, when compared with control HEK293-ACE2 cells (Fig. 2C, right). Taken together, these data show seemingly opposite phenotypes of resistance and susceptibility to SARS-CoV-2 infection in *STIM1*$^{-/-}$ and *ORAI1*$^{-/-}$ cells, respectively.

STIM1 KO cells exhibit resistance to SARS-CoV-2 infection as a result of higher baseline IFN-I response

Based on our previous data showing preactivation of the IFN-I pathway in *Stim1*$^{-/-}$ fibroblasts and macrophages (20) and high sensitivity of SARS-CoV-2 to IFN-I (10–12), we surmised that the resistance of *STIM1*$^{-/-}$ cells to SARS-CoV-2 infection was most likely derived from an increase in the baseline IFN-I response. As expected, *STIM1*$^{-/-}$ HEK293-ACE2 cells indeed showed higher

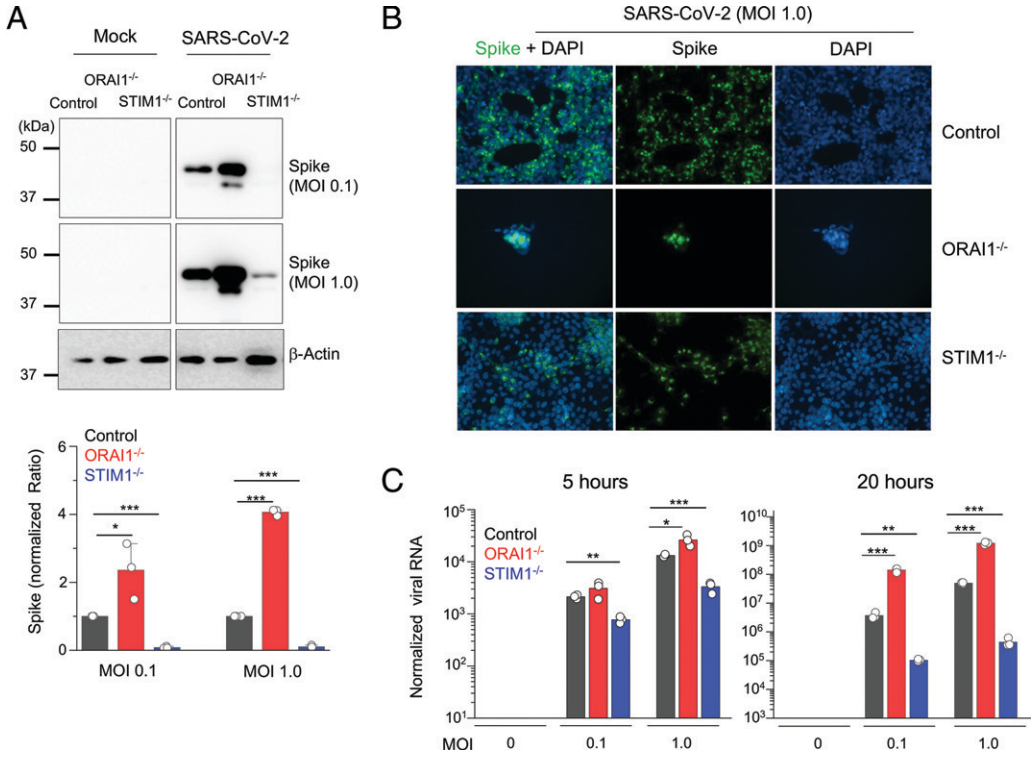

FIGURE 2. Loss of ORAI1 or STIM1 affects cellular susceptibility to SARS-CoV-2 infection. (**A**) Representative immunoblot showing expression of SARS-CoV-2 proteins in indicated HEK293-ACE2 cells under mock conditions or postinfection with SARS-CoV-2 at indicated MOIs. β-Actin is the loading control. Bottom bar graph shows densitometry analysis of normalized ratio of SARS-CoV-2 Spike protein to β-actin (± SEM) from three independent experiments. (**B**) Representative epifluorescence images (from two independent experiments, 200× magnification) showing expression of spike protein (green) in control, *ORAI1*$^{-/-}$, or *STIM1*$^{-/-}$ HEK293-ACE2 cells postinfection with SARS-CoV-2 at MOI 1.0. Cells were costained with DAPI for detection of nuclei. *ORAI1*$^{-/-}$ HEK293-ACE2 cells were all detached because of high virus load. (**C**) Quantitative RT-PCR analysis of viral genome from indicated cell types under mock conditions or postinfection with SARS-CoV-2 at indicated MOI for 5 (left graph) or 20 (right graph) h. Shown is one representative triplicate from two independent experiments. $^{**}p < 0.005$, $^{***}p < 0.0005$ (two-tailed *t* test).

levels of baseline IFN-β levels, which remained elevated even after SARS-CoV-2 infection (Fig. 3A). We also observed enhanced IL-6 production by *STIM1*$^{-/-}$ cells under resting conditions and after SARS-CoV-2 infection when compared with control cells (Fig. 3B). Notably, these results showed that SARS-CoV-2 infection did not trigger a robust IFN-I response but induced strong IL-6 expression consistent with previous observations (36).

To validate whether the resistance of *STIM1*$^{-/-}$ cells to SARS-CoV-2 infection was due to elevated IFN-I signaling, we generated HEK293-ACE2 cells deleted for both *STIM1* and *IFNAR1* using the CRISPR-Cas9 genome editing system (Fig. 3C). Deletion of *IFNAR1* abolished the increased baseline IFN-β expression in *STIM1*$^{-/-}$ cells (Fig. 3D). In addition, codeletion of *IFNAR1* abolished the resistance of *STIM1*$^{-/-}$ cells to SARS-CoV-2, as demonstrated by enhanced expression of viral proteins and increased burden of viral genome copies (Fig. 3E). These results suggest that the strong resistance of *STIM1*$^{-/-}$ cells to SARS-CoV-2 is predominantly derived from enhanced basal level of IFN-β. Considering that SARS-CoV-2 did not trigger robust IFN-I signaling, these results also emphasize the importance of the basal IFN-I levels in host resistance to SARS-CoV-2 infection.

High susceptibility of ORAI1 KO cells to SARS-CoV-2 infection is due to low baseline IFN-I signaling

The increased susceptibility of *ORAI1*$^{-/-}$ cells to SARS-CoV-2 infection was surprising because ORAI1 deficiency did not influence host resistance to infection with a DNA virus, HSV type 1 (HSV-1), in a previous study (20). Because SARS-CoV-2 is highly sensitive to the baseline IFN-I levels as observed in our analysis of *STIM1*$^{-/-}$ cells, we hypothesized that ORAI1 may influence the basal IFN-I levels. Culture supernatant analysis showed almost complete abrogation of baseline IFN-β levels in *ORAI1*$^{-/-}$ cells when compared with control cells under resting conditions, as well as on infection with SARS-CoV-2 at low MOI (Fig. 4A). IL-6 levels in these cells were not influenced. In support of reduced IFN-β levels, *ORAI1*$^{-/-}$ cells also showed reduced activation of the tonic IFN-I signaling pathway, including reduced basal levels of p-STAT1, as well as decrease in total STAT1 proteins (Fig. 4B), which has been proposed to be dependent on tonic IFN-β signaling (17).

To check whether the high susceptibility of *ORAI1*$^{-/-}$ cells to SARS-CoV-2 infection was rescued by treatment with IFN-β, we pretreated these cells with low levels of IFN-β for ∼20 h before SARS-CoV-2 infection. IFN-β pretreatment reduced the viral genome by ∼10-fold in control cells, in agreement with other studies (10–12) (Fig. 4C). Importantly, pretreatment of *ORAI1*$^{-/-}$ cells with IFN-β made the cells highly resistant, with more than 1,000-fold reduction in viral genome copy number, similar to the levels observed with control cells. These observations were validated by immunoblotting to check expression of viral proteins, where pretreatment with IFN-β abrogated expression of viral proteins equally in control and *ORAI1*$^{-/-}$ cells (Fig. 4D). Because IFN-β pretreatment in *ORAI1*$^{-/-}$ cells almost completely rescued the phenotypes to the level in control cells, these data suggest that reduced IFN-I baseline may have a significant contribution toward high susceptibility of *ORAI1*$^{-/-}$ cells to SARS-CoV-2 infection. Because the NFAT family of transcription factors are well-known downstream effectors of ORAI1-mediated SOCE, we checked whether reduced IFN-β levels in *ORAI1*$^{-/-}$ cells were due to loss

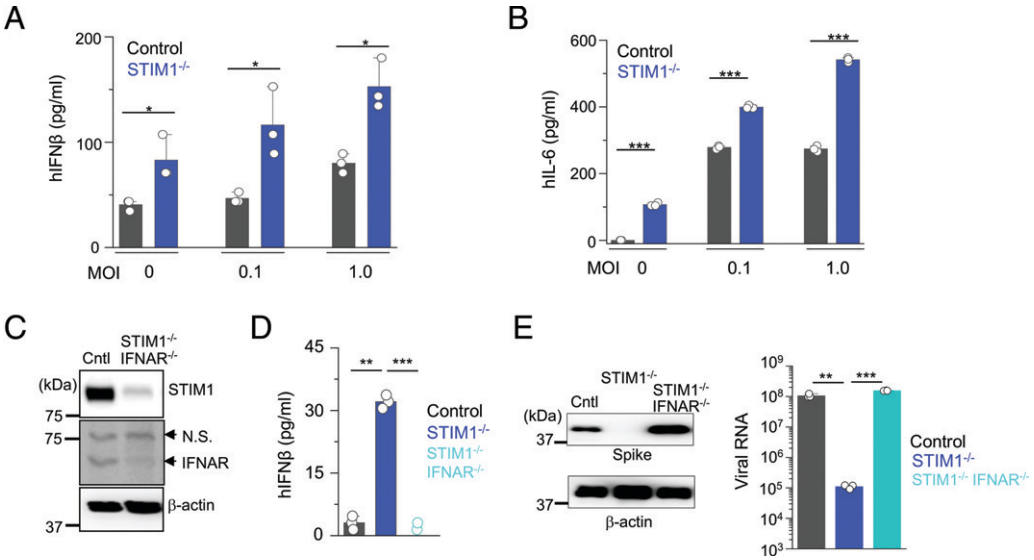

FIGURE 3. Loss of STIM1 imparts resistance to SARS-CoV-2 infection by enhancing the IFN-β signaling pathway. (**A**) Levels of IFN-β in culture supernatants from control or *STIM1*$^{-/-}$ HEK293-ACE2 cells under mock conditions or 20 h postinfection with SARS-CoV-2 at indicted MOIs. (**B**) Levels of IL-6 in culture supernatants from control or *STIM1*$^{-/-}$ HEK293-ACE2 cells. (**C**) Representative immunoblot showing expression of STIM1 and IFNAR1 in control HEK293-ACE2 cells or those deleted for both STIM1 and IFNAR1 using CRISPR-Cas9–mediated recombination. β-Actin is the loading control. Data are representative of two independent experiments. (**D**) Levels of IFN-β in culture supernatants from control, *STIM1*$^{-/-}$, or *STIM1*$^{-/-}$ *IFNAR*$^{-/-}$ HEK293-ACE2 cells under resting conditions. (**E**) Representative immunoblot showing expression of SARS-CoV-2 proteins in indicated HEK293-ACE2 cells under mock conditions or postinfection with SARS-CoV-2 at MOI of 0.1. β-Actin is the loading control. Data are representative of two independent infection experiments. (Right) Quantitative RT-PCR analysis of viral genome from indicated cell types under mock conditions or postinfection with SARS-CoV-2 at MOI 0.1 for 20 h. In bar graphs in panels (A), (B), (B), and (E), representative triplicates from two independent experiments are shown. $*p < 0.05$, $**p < 0.005$, $***p < 0.0005$ (two-tailed *t* test). N.S., nonspecific band.

of NFAT function. To check this possibility, we used CsA, which blocks calcineurin, a phosphatase necessary for dephosphorylation of NFAT in the cytoplasm. We pretreated control and *ORAI1*$^{-/-}$ HEK293-ACE2 cells with CsA and examined its effect on the basal IFN-β production. Surprisingly, CsA treatment did not affect IFN-β levels in either of these cell types, suggesting a potential role of Ca^{2+}-dependent transcription factors other than NFAT in this event (Fig. 4E).

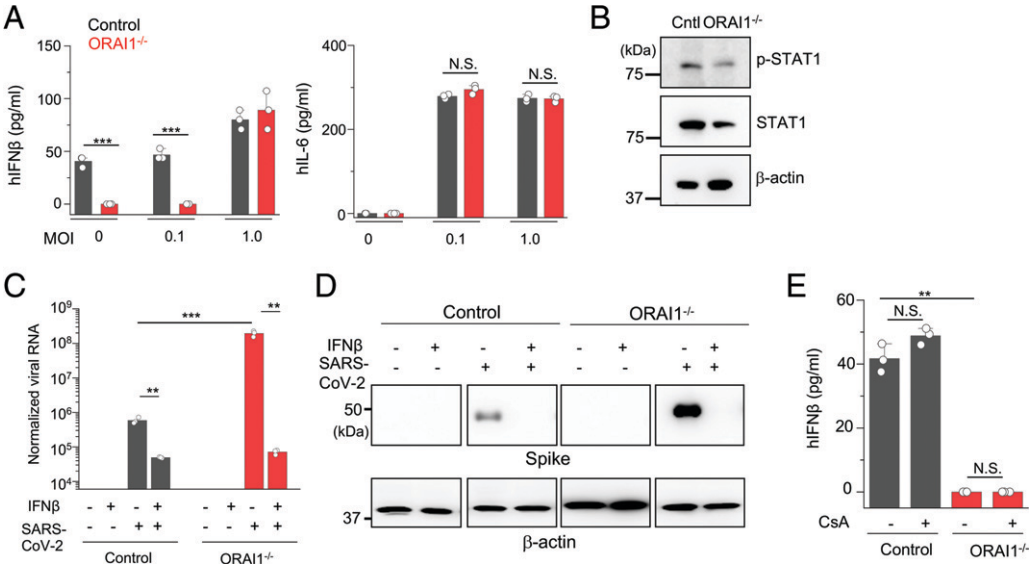

FIGURE 4. Loss of ORAI1 imparts susceptibility to SARS-CoV-2 infection by abrogating baseline IFN-β levels. (**A**) Levels of IFN-β and IL-6 in culture supernatants from control or *ORAI1*$^{-/-}$ HEK293-ACE2 cells under mock conditions or 20 h postinfection with SARS-CoV-2 at indicted MOIs. (**B**) Representative immunoblot showing expression of phosphorylated STAT1 (p-STAT1) or total STAT1 in lysates from control or *ORAI1*$^{-/-}$ HEK293-ACE2 cells. β-Actin is the loading control. Data are representative of three independent experiments. (**C**) Quantitative RT-PCR analysis of viral genome from indicated cell types with or without pretreatment with 100 U/ml IFN-β (for 20 h) under mock conditions or postinfection with SARS-CoV-2 at MOI 0.1 for 20 h. Data are representative of two independent infection experiments. (**D**) Representative immunoblot showing expression of SARS-CoV-2 proteins in indicated HEK293-ACE2 cells with or without pretreatment with 100 U/ml IFN-β (for 20 h) under mock conditions or postinfection with SARS-CoV-2 at MOI 0.1. β-Actin is the loading control. Data are representative of two independent infection experiments. (**E**) Levels of IFN-β in culture supernatants from control or *ORAI1*$^{-/-}$ HEK293-ACE2 cells with or without pretreatment with 1 μM CsA (20 h). In bar graphs in (A) and (E), representative triplicates from two independent experiments are shown. $**p < 0.005$, $***p < 0.0005$ (two-tailed *t* test).

ORAI1 acts on Ca^{2+}-regulated transcription factors to modulate the baseline IFN-I production

To uncover the antiviral defense mechanisms impaired in *ORAI1*$^{-/-}$ cells, we performed transcriptome analysis by bulk RNA-seq of control, *ORAI1*$^{-/-}$, and *STIM1*$^{-/-}$ HEK293-ACE2 cells before and 20 h after SARS-CoV-2 infection (Supplemental Fig. 2). Among infected samples, viral count analysis showed uniform increase in expression of all the viral genes in *ORAI1*$^{-/-}$ cells, whereas the same was uniformly reduced in *STIM1*$^{-/-}$ cells, when compared with control cells (Fig. 5A). Importantly, the viral genome reads comprised ∼20% of the total reads for control cells, ∼77% for *ORAI1*$^{-/-}$ cells, and <1% for *STIM1*$^{-/-}$ cells, in concurrence with the observed phenotypes (Fig. 5B). Pathway enrichment analysis of *ORAI1*$^{-/-}$ cells before infection showed downregulation of multiple antiviral defense mechanisms, including ISG15 antiviral mechanism and MyD88 signaling pathways (Fig. 5C–E). Transcriptome analysis further identified multiple transcription factors known to be involved in antiviral pathways, whose expression was altered by loss of *ORAI1* (Fig. 5F). Among the transcription factors that were significantly downregulated in *ORAI1*$^{-/-}$ cells, we identified *MEF2C* and members of the AP-1 family of transcription factors, *FOS*, *ATF2*, and *JUN*. All of these transcription factors are known to be Ca^{2+} dependent for their functions (37–40). The AP-1 family of transcription factors, including FOS, JUN, and ATF2, are known to bind the *IFNB* promoter to regulate its expression, and JUN is also known to mediate tonic IFN signaling (17). Remarkably, promoter analysis showed profound enrichment of FOS, ATF2, MEF2C, and JUN bindings sites among the DEGs in *ORAI1*$^{-/-}$ cells compared with the reference genome (Fig. 5G). Quantitative RT-PCR analysis confirmed downregulation of these transcription factors in *ORAI1*$^{-/-}$ cells under sterile conditions (Fig. 5H). Together, these data suggest that ORAI1 activity upregulates

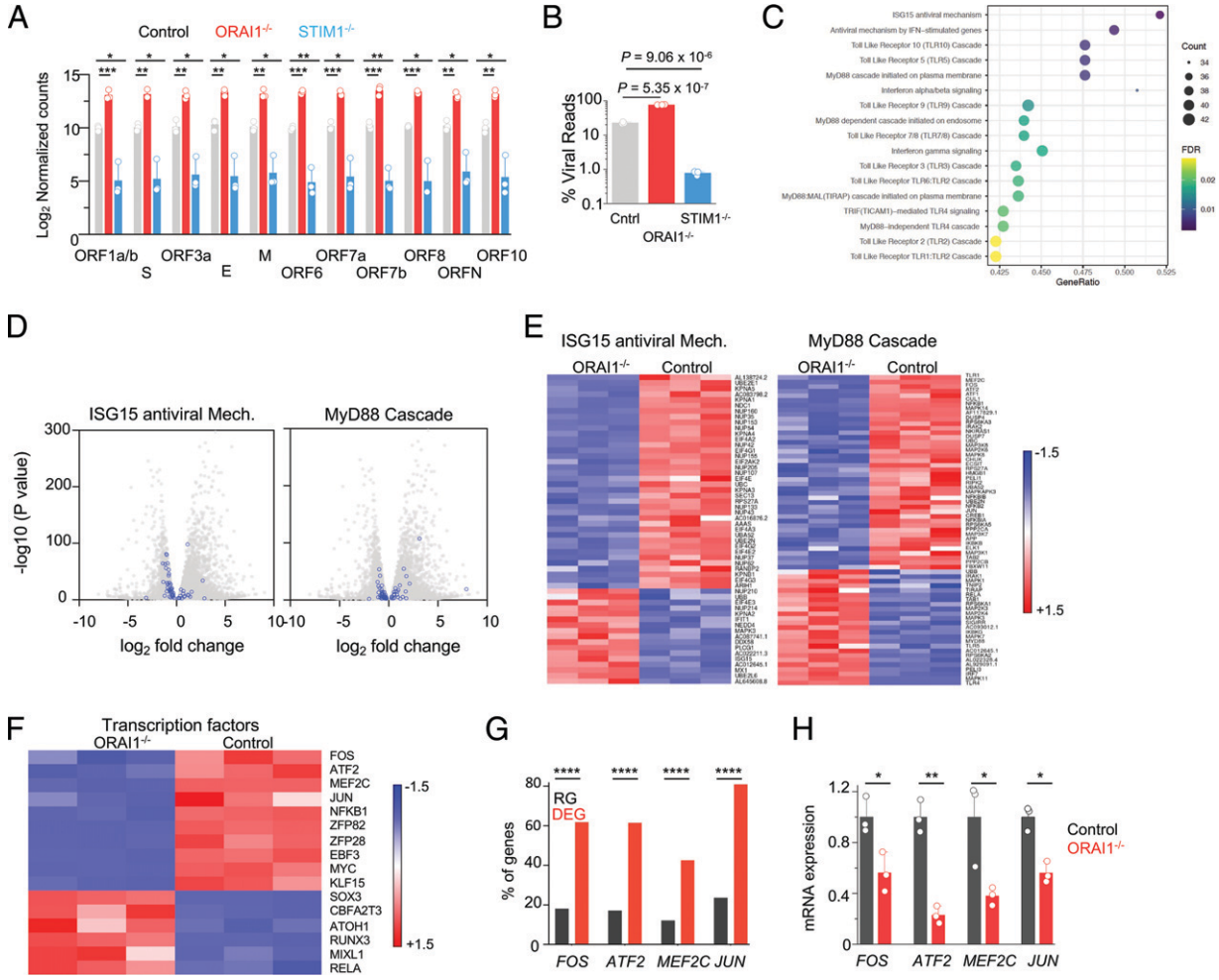

FIGURE 5. Transcriptome analysis of control and *ORAI1*$^{-/-}$ HEK293-ACE2 cells. (**A**) Normalized read counts (log_2) of SARS-CoV-2 RNA products, showing transcriptional enrichment of viral genes in SARS-CoV-2–infected cells when compared with uninfected cells. (**B**) Bar graph shows proportion of total reads comprising SARS-CoV-2 transcripts in indicated cell types. The proportion of virus-aligned reads over total reads is shown for each sample. Error bars represent average (± SD) from three biological replicates. (**C**) Dot plot visualization of enriched pathways in *ORAI1*$^{-/-}$ HEK293-ACE2 cells. Reactome pathway enrichment analysis was performed in PANTHER. The size of the dots represents the percentage of genes enriched in the total gene set, while its color represents the FDR (*p*-adjusted) value for each enriched pathway. (**D**) Volcano plots with all DEGs from *ORAI1*$^{-/-}$ and control mock (uninfected) samples in gray and the indicated gene sets of anti-viral ISG15 signaling (left) and MyD88 signaling (right) highlighted in blue (FDR < 0.01). (**E**) Heatmap illustrating *Z* scores as expression levels of the DEGs involved in antiviral signaling and MyD88 signaling pathways as show in (D). Blue and red colors represent downregulated and upregulated genes, respectively. (**F**) Heatmap depicting *Z* scores as expression levels of selected transcription factors differentially expressed between control and *ORAI1*$^{-/-}$ HEK293-ACE2 cells. (**G**) Transcription factor binding sites at the promoters of genes (transcription start site ± 1.0 kb) of the entire genome (from ChIP Atlas, RG) or among DEGs in *ORAI1*$^{-/-}$ HEK293-ACE2 cells. The hypergeometric *p* values (****$p <$ 0.0001) were calculated by comparing background (complete gene sets of the reference host) to genes from DEGs to see enrichment of binding sites of indicated transcription factors. (**H**) Quantitative RT-PCR analysis of the indicated genes from control and *ORAI1*$^{-/-}$ HEK293-ACE2 cells under resting conditions. *$p < 0.05$, **$p < 0.005$, ***$p < 0.0005$ (two-tailed *t* test).

expression of the transcription factors *MEF2C*, *FOS*, *ATF2*, and *JUN*, leading to induction of multiple genes involved in antiviral defense mechanisms, including those involved in tonic IFN-I signaling, providing resistance to SARS-CoV-2 infection.

Recent studies using genome-wide CRISPR-Cas9 KO screens with SARS-CoV-2 infection have identified a plethora of host factors important for productive infection by SARS-CoV-2 (41–45). The list of necessary host factors required for SARS-CoV-2 propagation varied widely among the different screens, likely because of different cell types and infection conditions used for each screen. Not surprisingly, all the genome-wide screens identified ACE2, the receptor for SARS-CoV-2, as an essential factor for virus propagation. Our transcriptome analysis identified many of these host factors among the DEGs in *ORAI1*$^{-/-}$ cells (Supplemental Fig. 3). However, many of these factors were downregulated in *ORAI1*$^{-/-}$ cells, suggesting they may not play a significant role in high susceptibility of *ORAI1*$^{-/-}$ cells to SARS-CoV-2 infection. Collectively, these results suggest that ORAI1-mediated Ca^{2+} signaling is mainly important for the regulation of tonic IFN-I levels, rather than host factors for SARS-CoV-2 infection.

Pharmacological alteration of baseline $[Ca^{2+}]_i$ modulates host resistance to SARS-CoV-2

Because SARS-CoV-2 infects the respiratory tract, we sought to validate our observations with human lung cells. We generated A549 cells stably expressing ACE2 and deleted for expression of ORAI1 using the CRISPR-Cas9 genome editing system (Fig. 6A). Transcript analysis confirmed reduced expression of *IFNB* in *ORAI1*$^{-/-}$ A549-ACE2 cells (Fig. 6B). Next, we infected control and *ORAI1*$^{-/-}$ A549-ACE2 cells with SARS-CoV-2 and examined expression of viral proteins, as well as quantified expression of viral genome. Similar to our observations with HEK293-ACE2 cells, loss of ORAI1 imparted susceptibility to SARS-CoV-2 infection even in A549 cells, albeit to a lesser extent (Fig. 6C, 6D).

Recent studies focusing on identifying therapies for COVID-19 have found beneficial effects of IFN administration, especially at early stages of the disease, to reduce the severity and mortality associated with SARS-CoV-2 infections (46, 47). To check whether pharmacological alteration of homeostatic $[Ca^{2+}]_i$ affects host resistance to SARS-CoV-2, we pretreated A549-ACE2 cells with various doses of a well-known blocker of ORAI1, BTP2 (chemical name: *N*-[4-[3,5-*Bis*(trifluoromethyl)-1*H*-pyrazol-1-yl]phenyl]-4-methyl-1,2,3-thiadiazole-5-carboxamide), for ∼24 h to reduce homeostatic $[Ca^{2+}]_i$. Transcript analysis confirmed reduced expression of *IFNB* in blocker-treated cells (Fig. 6E). Further, infection with SARS-CoV-2 showed increased viral protein expression and replication in cells treated with the ORAI1 blocker, in concurrence with our observations with *ORAI1*$^{-/-}$ cells (Fig. 6F, 6G). Importantly, enhancing baseline $[Ca^{2+}]$ by pretreatment with low doses of an ionophore, ionomycin, elevated *IFNB* expression and imparted resistance to subsequent SARS-CoV-2 infection (Fig. 6H–J). These data show that enhancing baseline $[Ca^{2+}]_i$ is sufficient to impart resistance to SARS-CoV-2 infection, most likely via boosting tonic IFN-I signaling.

Discussion

The role of Ca^{2+} signaling mediated by ORAI1 and STIM1 in adaptive immune cells (e.g., T and B cells) is well established (18, 19). Further, an earlier report suggested that loss of SOCE imparted susceptibility to IFN-I–induced cell death in Jurkat T cells (48). However, the function of this pathway in the host–pathogen responses in innate immunity is poorly understood. A recent study had identified an important function of STIM1 in regulating the cytosolic DNA-sensing pathway via direct interaction with STING independently from its role in Ca^{2+} signaling (20). This study demonstrates a key role of ORAI1 in regulating tonic IFN-β levels and thereby the host response to SARS-CoV-2 infection by modulation of homeostatic cytoplasmic $[Ca^{2+}]$. Collectively, these studies uncover novel functions of CRAC channel components in the innate immune system.

Loss of STIM1 provides strong resistance to infection with HSV-1 by enhancing IFN-I signaling (20). The observation of resistance to virus infections in *STIM1*$^{-/-}$ cells has been extended to this study using SARS-CoV-2. Abrogation of IFN-I signaling by codeletion of IFNAR1 reduced baseline IFN-β secretion and rendered *STIM1*$^{-/-}$ cells susceptible to SARS-CoV-2 infection, emphasizing the role of IFN-I in this resistance. Interestingly, loss of ORAI1 did not affect host resistance to HSV-1, most likely because the STING signaling pathway, which is predominantly important for sensing DNA viruses, was not impaired in *ORAI1*$^{-/-}$ cells (20). However, loss of ORAI1 resulted in very high susceptibility, specifically to SARS-CoV-2 infection. In concurrence, pharmacological inhibition of ORAI1 to reduce homeostatic $[Ca^{2+}]_i$ or enhancing homeostatic $[Ca^{2+}]_i$ by pretreatment with ionomycin modulated host susceptibility to SARS-CoV-2 infection. SARS-CoV-2 shows exceptionally high sensitivity to pretreatment with IFN-I or IFN-III, which profoundly reduces virus replication (10–12). Hence reduction in tonic IFN-β levels may enhance the susceptibility of *ORAI1*$^{-/-}$ cells, especially to SARS-CoV-2 infection. It has been shown that in the absence of priming amounts of IFN-β, mouse embryonic fibroblasts do not produce other IFN-I, suggesting that IFN-β is a master regulator for all IFN-I activities and presumably those mediated by IFN-III (49, 50). It has also been suggested that tonic IFN-β signaling is required to maintain adequate expression of STAT1 and STAT2; accordingly, the absence of tonic IFN-β signaling reduces basal STAT expression (17), similar to our observation with *ORAI1*$^{-/-}$ cells (Fig. 4B). Besides, loss of ORAI1 was shown to downregulate multiple pathways, including ISG antiviral signaling, TLR7/8 signaling, and MyD88 signaling cascades involved in RNA sensing. Collectively, loss of tonic IFN-I signaling in combination with impaired function of other antiviral signaling cascades is likely to contribute toward the exquisite sensitivity of *ORAI1*$^{-/-}$ cells to SARS-CoV-2.

The *IFNB* promoter contains four positive regulatory domains (PRDI–PRDIV), which are occupied by overlapping transcription factor complexes. IFN regulatory factor 3 (IRF3) and IRF7 bind PRDI and PRDIII, the NF-κB RelA-p50 heterodimer binds PRDII, and the AP-1 heterodimer of ATF-2 and c-Jun binds PRDIV. The binding of each of these components in the correct orientation and location results in activation of the *IFNB* promoter in response to virus infection (17). Tonic IFN-β expression is independent of IRF3 and IRF7 but instead depends on the c-Jun and NF-κB p50 subunit. *ORAI1*$^{-/-}$ cells showed reduced expression of multiple AP-1 family transcription factors, including ATF-2, FOS, and JUN, as well as the NF-κB p50 subunit, which are likely to contribute to reduced baseline IFN-β levels in these cells. Notably, although SOCE was abolished in both *ORAI1*$^{-/-}$ and *STIM1*$^{-/-}$ cells, the baseline $[Ca^{2+}]$ was reduced in only *ORAI1*$^{-/-}$ cells. Based on the previous finding that STIM2, which has a lower binding affinity to Ca^{2+} than STIM1, is crucial for regulation of homeostatic Ca^{2+} levels (35), it is expected that *STIM2*$^{-/-}$ cells may have lower tonic IFN-I signaling, and thereby high susceptibility to SARS-CoV-2 infection similar to *ORAI1*$^{-/-}$ cells. Another notable difference between ORAI1 and STIM1 deficiency is differential expression of IFN-β and IL-6. *STIM1*$^{-/-}$ cells showed enhanced expression of both of these cytokines, consistent with the observation that activation of the STING pathway upregulates expression of both IFN-β and IL-6 (20, 21). However, *ORAI1*$^{-/-}$ cells had normal expression of IL-6 but still showed high susceptibility to SARS-CoV-2 infection,

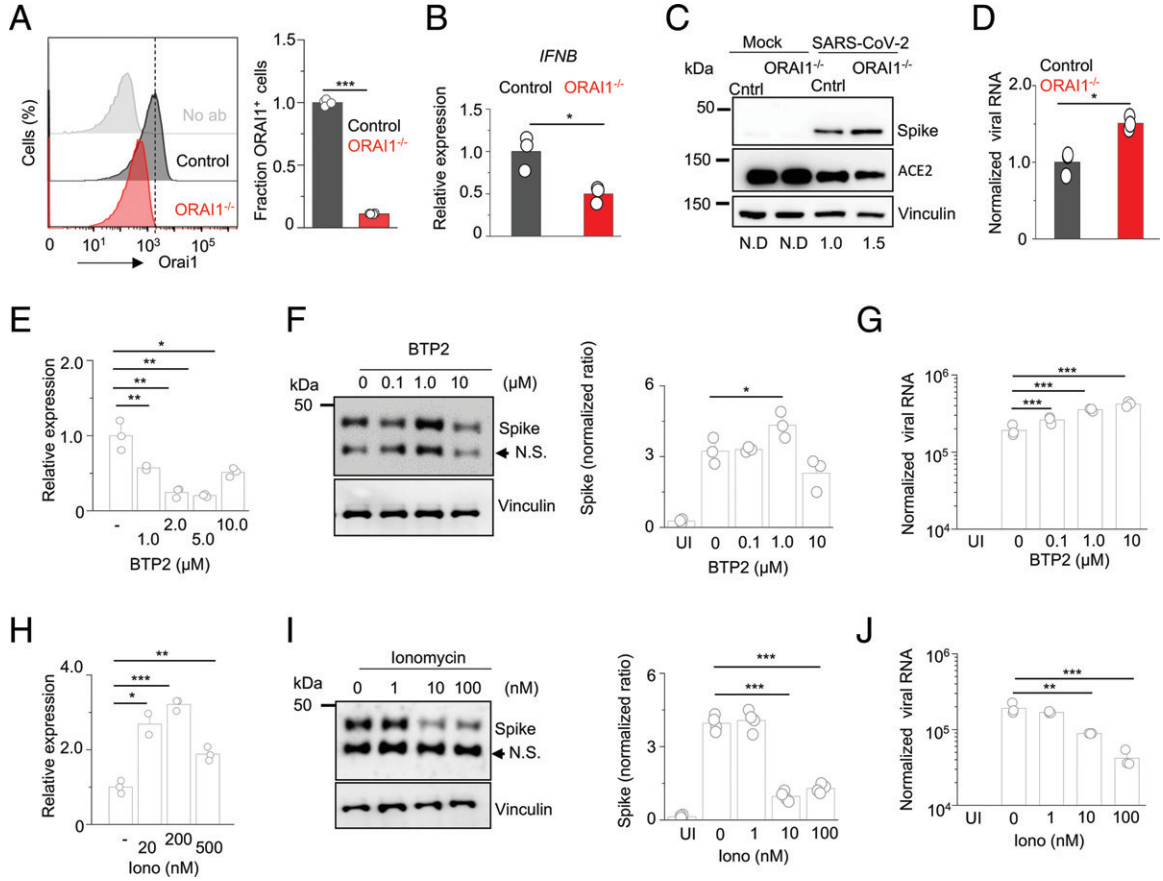

FIGURE 6. Pharmacological alteration of homeostatic $[Ca^{2+}]_i$ modulates host susceptibility to SARS-CoV-2. (**A**) Representative histograms showing levels of total ORAI1 protein in control and *ORAI1*$^{-/-}$ A549-ACE2 cells after permeabilization and intracellular staining with anti-ORAI1 Ab. The bar graph shows average (± SEM) from three independent experiments. (**B**) Quantitative RT-PCR analysis for expression of *IFNB* transcripts in control or *ORAI1*$^{-/-}$ A549-ACE2 cells cultured in the presence of medium containing 10 mM $CaCl_2$. Data are representative of two independent experiments. (**C**) Representative immunoblot showing expression of SARS-CoV-2 and ACE2 proteins in indicated A549-ACE2 cells under mock conditions or postinfection with SARS-CoV-2 at indicated MOI 0.1. Vinculin is the loading control. Numbers below indicate normalized fold change in ratio of Spike to vinculin. Data are representative of two experiments. (**D**) Quantitative RT-PCR analysis of viral genome from indicated A549-ACE2 cells postinfection with SARS-CoV-2 at MOI of 0.1 for 20 h. Data are representative of two experiments. (**E**) Quantitative RT-PCR analysis for expression of *IFNB* transcripts from A549-ACE2 cells pretreated with vehicle or indicated concentrations of BTP2 for 24 h. Shown is one representative triplicate from two independent experiments. (**F**) Representative immunoblot showing expression of SARS-CoV-2 proteins in A549-ACE2 cells pretreated with vehicle or indicated concentrations of ORAI1 blocker BTP2 for ∼24 h and infected with SARS-CoV-2 at MOI 0.1. Vinculin is the loading control. Bar graph (right) shows densitometry analysis of normalized ratio of SARS-N-CoV-2 to vinculin (± SEM) from technical replicates of two independent experiments. (**G**) Quantitative RT-PCR analysis of viral genome from A549-ACE2 cells pretreated with vehicle or indicated concentrations of ORAI1 blocker BTP2 for 24 h and infected with SARS-CoV-2 at MOI 0.1. Shown is one representative triplicate from two independent experiments. (**H**) Quantitative RT-PCR analysis for expression of *IFNB* transcripts from A549-ACE2 cells pretreated with vehicle or indicated concentrations of ionomycin (iono) for 24 h. Shown is one representative triplicate from two independent experiments. (**I**) Representative immunoblot showing expression of SARS-CoV-2 proteins in A549-ACE2 cells pretreated with vehicle or indicated concentrations of ionomycin for 24 h and infected with SARS-CoV-2 at MOI 0.1. Vinculin is the loading control. Bar graph (right) shows densitometry analysis of normalized ratio of SARS-N-CoV-2 to vinculin (± SEM) from technical replicates of two independent experiments. (**J**) Quantitative RT-PCR analysis of viral genome from A549-ACE2 cells pretreated with vehicle or indicated concentrations of ionomycin for 24 h and infected with SARS-CoV-2 at MOI 0.1. Shown is one representative triplicate from two independent experiments. $*p < 0.05$, $**p < 0.005$, $***p < 0.0005$ (two-tailed *t* test). N.D., not determined; N.S., nonspecific band; UI, uninfected cells.

suggesting that the protective effect of STIM1 deficiency is predominantly derived from increased levels of IFN-β. Therefore, these results obtained from the analysis of *ORAI1*$^{-/-}$ and *STIM1*$^{-/-}$ cells cohesively suggest that tonic IFN-I signaling is a crucial determinant for the degree of host resistance to SARS-CoV-2.

In summary, we examined the role of CRAC channel components, ORAI1 and STIM1, in host resistance to SARS-CoV-2 infection. *STIM1*$^{-/-}$ cells showed remarkable resistance to SARS-CoV-2 infection, supporting previous studies of the role of elevated baseline IFN-I levels (20). Loss of ORAI1 severely impaired the tonic IFN-I levels, thereby reducing resistance to SARS-CoV-2 infection. Mechanistically, ORAI1-mediated Ca^{2+} signaling affects expression of various transcription factors, including *FOS*, *JUN*, *ATF2*, and *MEF2C*, that regulate multiple host defense pathways. The key finding of this study is that the baseline IFN-β level regulated by ORAI1-mediated Ca^{2+} signaling is critical for priming the cellular antiviral state, thereby determining host resistance to SARS-CoV-2 infection. A recent phase 2 clinical trial of inhaled, nebulized IFN-β to treat people with COVID-19 resulted in accelerated recovery, supporting localized delivery of IFN-I as a potential prophylactic and therapeutic agent against COVID-19 (47). The therapeutic effect of IFN-I targeting SARS-CoV-2 infection may be partly derived from boosting tonic IFN-I signaling. Our findings may help develop novel therapeutic methods to combat SARS-CoV-2 infection by

demonstrating that pharmacological enhancement of baseline cytoplasmic [Ca^{2+}] improved host resistance to SARS-CoV-2. Furthermore, the current study emphasizing the crucial role of tonic IFN-I signaling in resistance to SARS-CoV-2 infection may guide future identification of vulnerable populations and targeted therapies at boosting tonic IFN-I signaling.

Acknowledgments

We thank Barbara Dillon, UCLA High-Containment Program Director, for BSL3 work. We also thank Yousang Gwack (UCLA) for helpful suggestions and Shawn Cokus (UCLA Collaboratory Fellow) for suggestions about statistical analysis of transcription factor enrichment data.

Disclosures

The authors have no financial conflicts of interest.

References

1. tenOever, B. R. 2016. The evolution of antiviral defense systems. *Cell Host Microbe* 19: 142–149.
2. Iwasaki, A., and R. Medzhitov. 2015. Control of adaptive immunity by the innate immune system. *Nat. Immunol.* 16: 343–353.
3. Lazear, H. M., J. W. Schoggins, and M. S. Diamond. 2019. Shared and distinct functions of type I and type III interferons. *Immunity* 50: 907–923.
4. Crotta, S., S. Davidson, T. Mahlakoiv, C. J. Desmet, M. R. Buckwalter, M. L. Albert, P. Staeheli, and A. Wack. 2013. Type I and type III interferons drive redundant amplification loops to induce a transcriptional signature in influenza-infected airway epithelia. *PLoS Pathog.* 9: e1003773.
5. Schulz, K. S., and K. L. Mossman. 2016. Viral evasion strategies in type I IFN signaling – a summary of recent developments. *Front. Immunol.* 7: 498.
6. Xia, H., and P. Y. Shi. 2020. Antagonism of type I interferon by severe acute respiratory syndrome coronavirus 2. *J. Interferon Cytokine Res.* 40: 543–548.
7. Xie, M., and Q. Chen. 2020. Insight into 2019 novel coronavirus – an updated interim review and lessons from SARS-CoV and MERS-CoV. *Int. J. Infect. Dis.* 94: 119–124.
8. Bastard, P., L. B. Rosen, Q. Zhang, E. Michailidis, H.-H. Hoffmann, Y. Zhang, K. Dorgham, Q. Philippot, J. Rosain, V. Béziat, et al. 2020. Autoantibodies against type I IFNs in patients with life-threatening COVID-19. *Science* 370: eabd4585.
9. Zhang, Q., P. Bastard, Z. Liu, J. Le Pen, M. Moncada-Velez, J. Chen, M. Ogishi, I. K. D. Sabli, S. Hodeib, C. Korol, et al. 2020. Inborn errors of type I IFN immunity in patients with life-threatening COVID-19. *Science* 370: eabd4570.
10. Vanderheiden, A., P. Ralfs, T. Chirkova, A. A. Upadhyay, M. G. Zimmerman, S. Bedoya, H. Aoued, G. M. Tharp, K. L. Pellegrini, C. Manfredi, et al. 2020. Type I and type III interferons restrict SARS-CoV-2 infection of human airway epithelial cultures. *J. Virol.* 94: e00985-20.
11. Lokugamage, K. G., A. Hage, M. de Vries, A. M. Valero-Jimenez, C. Schindewolf, M. Dittmann, R. Rajsbaum, and V. D. Menachery. 2020. Type I interferon susceptibility distinguishes SARS-CoV-2 from SARS-CoV. *J. Virol.* 94: e01410-20.
12. Blanco-Melo, D., B. E. Nilsson-Payant, W. C. Liu, S. Uhl, D. Hoagland, R. Møller, T. X. Jordan, K. Oishi, M. Panis, D. Sachs, et al. 2020. Imbalanced host response to SARS-CoV-2 drives development of COVID-19. *Cell* 181: 1036–1045.e9.
13. Humphries, F., L. Shmuel-Galia, Z. Jiang, R. Wilson, P. Landis, S.-L. Ng, K.-M. Parsi, R. Maehr, J. Cruz, A. Morales-Ramos, et al. 2021. A diamidobenzimidazole STING agonist protects against SARS-CoV-2 infection. *Sci. Immunol.* 6: eabi9002.
14. Li, M. F., M. Ferretti, B. Ying, H. Descamps, E. Lee, M. Dittmar, J. S. Lee, K. Whig, B. Kamalia, L. Dohnalová, et al. 2021. Pharmacological activation of STING blocks SARS-CoV-2 infection. *Sci. Immunol.* 6: eabi9007.
15. Liu, W., H. M. Reyes, J. F. Yang, Y. Li, K. M. Stewart, M. C. Basil, S. M. Lin, J. Katzen, E. E. Morrisey, S. R. Weiss, and J. You. 2021. Activation of STING signaling pathway effectively blocks human coronavirus infection. *J. Virol.* 95: e00490-21.
16. Zhu, Q., Y. Zhang, L. Wang, X. Yao, D. Wu, J. Cheng, X. Pan, H. Liu, Z. Yan, and L. Gao. 2021. Inhibition of coronavirus infection by a synthetic STING agonist in primary human airway system. *Antiviral Res.* 187: 105015.
17. Gough, D. J., N. L. Messina, C. J. Clarke, R. W. Johnstone, and D. E. Levy. 2012. Constitutive type I interferon modulates homeostatic balance through tonic signaling. *Immunity* 36: 166–174.
18. Srikanth, S., and Y. Gwack. 2013. Orai1-NFAT signalling pathway triggered by T cell receptor stimulation. *Mol. Cells* 35: 182–194.
19. Prakriya, M., and R. S. Lewis. 2015. Store-operated calcium channels. *Physiol. Rev.* 95: 1383–1436.
20. Srikanth, S., J. S. Woo, B. Wu, Y. M. El-Sherbiny, J. Leung, K. Chupradit, L. Rice, G. J. Seo, G. Calmettes, C. Ramakrishna, et al. 2019. The Ca^{2+} sensor STIM1 regulates the type I interferon response by retaining the signaling adaptor STING at the endoplasmic reticulum. *Nat. Immunol.* 20: 152–162.
21. Hopfner, K. P., and V. Hornung. 2020. Molecular mechanisms and cellular functions of cGAS-STING signalling. *Nat. Rev. Mol. Cell Biol.* 21: 501–521.
22. Rice, L., C. Stockdale, I. Berry, S. O'Riordan, K. Pysden, R. Anwar, R. Rushambuza, M. Blyth, S. Srikanth, Y. Gwack, et al. 2019. A report of novel STIM1 deficiency and 6-year follow-up of two previous cases associated with mild immunological phenotype. *J. Clin. Immunol.* 39: 249–256.
23. Garcia, G., Jr., A. Sharma, A. Ramaiah, C. Sen, A. Purkayastha, D. B. Kohn, M. S. Parcells, S. Beck, H. Kim, M. A. Bakowski, et al. 2021. Antiviral drug screen identifies DNA-damage response inhibitor as potent blocker of SARS-CoV-2 replication. *Cell Rep.* 35: 108940.
24. Srikanth, S., H. J. Jung, B. Ribalet, and Y. Gwack. 2010. The intracellular loop of Orai1 plays a central role in fast inactivation of Ca2+ release-activated Ca2+ channels. *J. Biol. Chem.* 285: 5066–5075.
25. Srikanth, S., H. J. Jung, K. D. Kim, P. Souda, J. Whitelegge, and Y. Gwack. 2010. A novel EF-hand protein, CRACR2A, is a cytosolic Ca2+ sensor that stabilizes CRAC channels in T cells. *Nat. Cell Biol.* 12: 436–446.
26. Dobin, A., C. A. Davis, F. Schlesinger, J. Drenkow, C. Zaleski, S. Jha, P. Batut, M. Chaisson, and T. R. Gingeras. 2013. STAR: ultrafast universal RNA-seq aligner. *Bioinformatics* 29: 15–21.
27. Love, M. I., W. Huber, and S. Anders. 2014. Moderated estimation of fold change and dispersion for RNA-seq data with DESeq2. *Genome Biol.* 15: 550.
28. Marini, F., and H. Binder. 2019. pcaExplorer: an R/Bioconductor package for interacting with RNA-seq principal components. *BMC Bioinformatics* 20: 331.
29. Jassal, B., L. Matthews, G. Viteri, C. Gong, P. Lorente, A. Fabregat, K. Sidiropoulos, J. Cook, M. Gillespie, R. Haw, et al. 2020. The reactome pathway knowledgebase. *Nucleic Acids Res.* 48(D1): D498–D503.
30. Khomtchouk, B. B., J. R. Hennessy, and C. Wahlestedt. 2017. shinyheatmap: Ultra fast low memory heatmap web interface for big data genomics. *PLoS One* 12: e0176334.
31. Oki, S., T. Ohta, G. Shioi, H. Hatanaka, O. Ogasawara, Y. Okuda, H. Kawaji, R. Nakaki, J. Sese, and C. Meno. 2018. ChIP-Atlas: a data-mining suite powered by full integration of public ChIP-seq data. *EMBO Rep.* 19: e46255.
32. Li, W., M. J. Moore, N. Vasilieva, J. Sui, S. K. Wong, M. A. Berne, M. Somasundaran, J. L. Sullivan, K. Luzuriaga, T. C. Greenough, et al. 2003. Angiotensin-converting enzyme 2 is a functional receptor for the SARS coronavirus. *Nature* 426: 450–454.
33. Nomura, A., S. Yokoe, K. Tomoda, T. Nakagawa, F. J. Martin-Romero, and M. Asahi. 2020. Fluctuation in *O*-GlcNAcylation inactivates STIM1 to reduce store-operated calcium ion entry via down-regulation of Ser^{621} phosphorylation. *J. Biol. Chem.* 295: 17071–17082.
34. Yoast, R. E., S. M. Emrich, X. Zhang, P. Xin, M. T. Johnson, A. J. Fike, V. Walter, N. Hempel, D. I. Yule, J. Sneyd, et al. 2020. The native ORAI channel trio underlies the diversity of Ca^{2+} signaling events. *Nat. Commun.* 11: 2444.
35. Brandman, O., J. Liou, W. S. Park, and T. Meyer. 2007. STIM2 is a feedback regulator that stabilizes basal cytosolic and endoplasmic reticulum Ca2+ levels. *Cell* 131: 1327–1339.
36. Chen, G., D. Wu, W. Guo, Y. Cao, D. Huang, H. Wang, T. Wang, X. Zhang, H. Chen, H. Yu, et al. 2020. Clinical and immunological features of severe and moderate coronavirus disease 2019. *J. Clin. Invest.* 130: 2620–2629.
37. Ng, S. W., C. Nelson, and A. B. Parekh. 2009. Coupling of Ca(2+) microdomains to spatially and temporally distinct cellular responses by the tyrosine kinase Syk. *J. Biol. Chem.* 284: 24767–24772.
38. McKinsey, T. A., C. L. Zhang, and E. N. Olson. 2002. MEF2: a calcium-dependent regulator of cell division, differentiation and death. *Trends Biochem. Sci.* 27: 40–47.
39. Lesch, A., X. Hui, P. Lipp, and G. Thiel. 2015. Transient receptor potential melastatin-3 (TRPM3)-induced activation of AP-1 requires Ca2+ ions and the transcription factors c-Jun, ATF2, and ternary complex factor. *Mol. Pharmacol.* 87: 617–628.
40. Ban, N., Y. Yamada, Y. Someya, Y. Ihara, T. Adachi, A. Kubota, R. Watanabe, A. Kuroe, A. Inada, K. Miyawaki, et al. 2000. Activating transcription factor-2 is a positive regulator in CaM kinase IV-induced human insulin gene expression. *Diabetes* 49: 1142–1148.
41. Hoffmann, H. H., W. M. Schneider, K. Rozen-Gagnon, L. A. Miles, F. Schuster, B. Razooky, E. Jacobson, X. Wu, S. Yi, C. M. Rudin, et al. 2021. TMEM41B is a *Pan*-flavivirus host factor. *Cell* 184: 133–148.e20.
42. Schneider, W. M., J. M. Luna, H. H. Hoffmann, F. J. Sánchez-Rivera, A. A. Leal, A. W. Ashbrook, J. Le Pen, I. Ricardo-Lax, E. Michailidis, A. Peace, et al. 2021. Genome-scale identification of SARS-CoV-2 and *Pan*-coronavirus host factor networks. *Cell* 184: 120–132.e14.
43. Wang, R., C. R. Simoneau, J. Kulsuptrakul, M. Bouhaddou, K. A. Travisano, J. M. Hayashi, J. Carlson-Stevermer, J. R. Zengel, C. M. Richards, P. Fozouni, et al. 2021. Genetic screens identify host factors for SARS-CoV-2 and common cold coronaviruses. *Cell* 184: 106–119.e14.
44. Wei, J., M. M. Alfajaro, P. C. DeWeirdt, R. E. Hanna, W. J. Lu-Culligan, W. L. Cai, M. S. Strine, S. M. Zhang, V. R. Graziano, C. O. Schmitz, et al. 2021. Genome-wide CRISPR screens reveal host factors critical for SARS-CoV-2 infection. *Cell* 184: 76–91.e13.
45. Daniloski, Z., T. X. Jordan, H. H. Wessels, D. A. Hoagland, S. Kasela, M. Legut, S. Maniatis, E. P. Mimitou, L. Lu, E. Geller, et al. 2021. Identification of required host factors for SARS-CoV-2 infection in human cells. *Cell* 184: 92–105.e16.
46. Hoagland, D. A., R. Møller, S. A. Uhl, K. Oishi, J. Frere, I. Golynker, S. Horiuchi, M. Panis, D. Blanco-Melo, D. Sachs, et al. 2021. Leveraging the antiviral type I interferon system as a first line of defense against SARS-CoV-2 pathogenicity. *Immunity* 54: 557–570.e5.
47. Monk, P. D., R. J. Marsden, V. J. Tear, J. Brookes, T. N. Batten, M. Mankowski, F. J. Gabbay, D. E. Davies, S. T. Holgate, L. P. Ho, et al.; Inhaled Interferon Beta COVID-19 Study Group. 2021. Safety and efficacy of inhaled nebulised

interferon beta-1a (SNG001) for treatment of SARS-CoV-2 infection: a randomised, double-blind, placebo-controlled, phase 2 trial. *Lancet Respir. Med.* 9: 196–206.
48. Yue, C., J. Soboloff, and A. M. Gamero. 2012. Control of type I interferon-induced cell death by Orai1-mediated calcium entry in T cells. *J. Biol. Chem.* 287: 3207–3216.
49. Takaoka, A., Y. Mitani, H. Suemori, M. Sato, T. Yokochi, S. Noguchi, N. Tanaka, and T. Taniguchi. 2000. Cross talk between interferon-gamma and -alpha/beta signaling components in caveolar membrane domains. *Science* 288: 2357–2360.
50. Erlandsson, L., R. Blumenthal, M. L. Eloranta, H. Engel, G. Alm, S. Weiss, and T. Leanderson. 1998. Interferon-beta is required for interferon-alpha production in mouse fibroblasts. *Curr. Biol.* 8: 223–226.